Inorg. Chem. **2005**, *44*, 8044–8052

BTA Copper Complexes

Manfred Friedrich,[§] Juan Carlos Gálvez-Ruiz,[†] Thomas M. Klapötke,*[,†] Peter Mayer,[†] Birgit Weber,[†] and Jan J. Weigand*[,†]

Department of Chemistry and Biochemistry, Ludwig-Maximilian University Munich Butenandtstrasse 5-13 (Haus D), 81377 Munich, Germany, and Institute of Inorganic and Analytical Chemistry, University of Jena, August-Bebel-Strasse 2, D-07743 Jena, Germany

Received April 28, 2005

Cupric oxide is one of the most important additives used (a) to catalyze decomposition reactions in gas generators to obtain cooler reaction gases, (b) as burning enhancer for ammonium perchlorate-based composite *propellants*, and (c) as coloring agent in *pyrotechnics*. In this context, the reaction of Cu^{2+} ions in aqueous ammonia solution with bis(tetrazolyl)amine (H_2bta**)** was investigated. Depending on the reaction conditions three complexes were obtained: $Cu(bta)(NH_3)_2$ (**1**), $Cu(bta)(NH_3)_2 \cdot H_2O$ (**2**), and $(NH_4)_2Cu(bta)_2 \cdot 2.5H_2O$ (**3**). The crystal structures of **1** and **2** are discussed with respect to the coordination mode of the dianion of *N*,*N*-bis(1(2)*H*-tetrazol-5-yl)-amine (bta), which mediates in the case of **1** and **2** weak superexchange interactions between the adjacent magnetic transition-metal Cu^{II} cations. These antiferromagnetic interactions result from 1D copper chains over an hidden azide end-to-end bridge. Interestingly, the structural arrangement of **1** completely changes in the presence of crystal-bound water. Moreover, some physicochemical properties (e.g., heat of formation, friction, and impact sensitivity, DSC) of these complexes with respect to high-energetic materials are discussed.

Introduction

Neutral as well ionic azides undergo cycloaddition with cyanogroups yielding a huge variety of different tetrazole derivatives, an increasingly popular functionality with wide-ranging applications.[1] The wide-spread interest in those compounds is not only found in pharmaceuticals, such as lipophilic spacers and carboxylic acid surrogates,[2] and in photography and information recording systems[3] but are also gaining increasing interest as explosives.[4] Complexes of CN species with transition metals are well-known and often exhibit interesting magnetic properties and are of interest for materials science.[5] An interesting precursor for cycloaddition reactions with azide, as an example of such a CN species, is the nonlinear pseudohalide dicyanamide anion ($N(CN)_2^-$), which exhibits a rich variety of bonding modes for coordination in (e.g., 3d complexes). Dicyanamide complexes have attracted much interest in recent years in the construction of supramolecular aggregates because of their intriguing network topologies and potential function as new class of materials.[6]

* To whom correspondence should be addressed. E-mail: tmk@cup.uni.muenchen.de. Fax: +49-89-2180-77492. Phone: +49-89-2180-77491.

† Ludwig-Maximilian University Munich.

§ University of Jena.

(1) Butler, R. N. In *Comprehensive Heterocyclic Chemistry*; Katritzky, A. R., Rees, C. W., Scriven, E. F. V., Eds.; Pergamon: Oxford, U.K., 1996; Vol. 4.

(2) Singh, H.; Chawla, A. S.; Kapoor, V. K.; Paul, D.; Malhotra, R. K. *Prog. Med. Chem.* **1980**, *17*, 151.

(3) Koldobskii, G. I.; Ostrovskii, V. A. *Usp. Khim.* **1994**, *63*, 847.

(4) (a) Ostrovskii, V. A.; Pevzner, M. S.; Kofmna, T. P.; Shcherbinin, M. B.; Tselinskii, I. V. *Targets Heterocycl. Syst.* **1999**, *3*, 467. (b) Hiskey, M.; Chavez, D. E.; Naud, D. L.; Son, S. F.; Berghout, H. L.; Bome, C. A. *Proc. Int. Pyrotech. Semin.* **2000**, *27*, 3.

(5) (a) Miller, J. S.; Epstein, A. J.; Reiff, W. M. *Acc. Chem. Res.* **1988**, *21*, 114. Miller, J. S.; Epstein, A. J.; Reiff, W. M. *Science* **1988**, *240*, 40. (b) Miller, J. S.; Epstein, A. J.; Reiff, W. M. *Chem. Rev.* **1988**, *88*, 201. (c) Miller, J. S.; Epstein, A. J. In *New Aspects of Organic Chemistry*; Yoshida, Z., Shiba, T., Ohsiro, Y., Eds.; VCH Publishers: New York, 1989; Vol. 237. (d) Miller, J. S.; Epstein, A. J. *Angew. Chem., Int. Ed. Engl.* **1994**, *33*, 385; *Angew. Chem.* **1994**, *106*, 399. (e) Miller, J. S.; Epstein, A. J. *Adv. Chem. Ser.* **1995**, *245*, 161. (f) Gadet, V.; Mallah, T.; Castro, I.; Verdaguer, M. *J. Am. Chem. Soc.* **1992**, *114*, 9213. (g) Mallah, T.; Ferlay, S.; Auberger, C.; Helary, C.; L'Hermite, F.; Ouahes, F.; Vaissermann, J.; Verdaguer, M.; Veillet, P. *Mol. Cryst., Liq. Cryst.* **1995**, *273*, 141. (h) Ferlay, S.; Mallah, T.; Ouahes, R.; Veillet, P.; Verdaguer, M. *Nature* **1995**, *378*, 701. (i) Entley, W. R.; Girolami, G. S. *Science* **1995**, *268*, 397. (j) Entley, W. R.; Girolami, G. S. *Inorg. Chem.* **1994**, *33*, 5165. (k) Entley, W. R.; Treadway, C. R.; Girolami, G. S. *Mol. Cryst., Liq. Cryst.* **1995**, *273*, 153. (l) Manson, J. L.; Kmety, C. R.; Huang, Q.; Lynn, J. W.; Bendele, G. B.; Pagola, S.; Stephens, P. W.; Liable-Sands, L. M.; Rheingold, A. L.; Epstein, A. J.; Miller, J. S. *Chem. Mater.* **1998**, *10*, 2552.

(6) (a) Eddaoudi, M.; Kim, J.; Rosi, N.; Vodak, D.; Wachter, J.; O'Keeffe, M.; Yaghi, O. M. *Science* **2002**, *295*, 469. (b) Li, H.; Eddaoudi, M.; O'Keeffe, M.; Yaghi, O. M. *Nature* **1999**, *402*, 276. (c) Batten, S. R.; Jensen, P.; Moubaraki, B.; Murray, K. S.; Robson, R. *Chem. Commun.* **1998**, 439.

10.1021/ic050657r CCC: $30.25
Published on Web 09/22/2005

Scheme 1. H_2bta with Two Reversible Types of Protonated and Deprotonated Mode

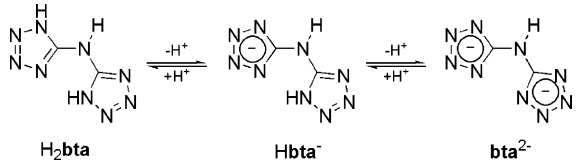

The reaction of sodium dicyanamide with sodium azide under acid-catalyzed conditions yields the corresponding *N*,*N*-bis(1(2)*H*-tetrazol-5-yl)-amine as a monohydrate ($H_2bta \cdot H_2O$).[7] Since, in the continuous search of novel energetic materials with high nitrogen content for applications such as low-smoke producing pyrotechnic compositions, gas generators, propellants, primers in primer charges (PC), and especially, high-energy-capacity transition-metal complexes, H_2bta might play an important role in future investigations, as well as in applications. The most promising high-energy materials, suitable for this purpose may be derived from, for example, 5-aminotetrazole (5-Hat) and its derivatives, *N*,*N*-bis-(1(2)*H*-tetrazol-5-yl)-amine monohydrate ($H_2bta \cdot H_2O$) or 5,5′-bis-1*H*-tetrazole (H_2bt).[8]

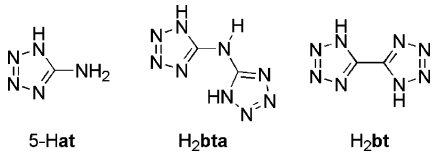

As *N*,*N*-bis-(1(2)*H*-tetrazol-5-yl)-amine (H_2bta) is a bidentate chelating ligand with multi-proton donor sites, it is able to coordinate to a metal with three reversible types of protonated and deprotonated modes: neutral (H_2bta), monodeprotonated (monoanion, $Hbta^-$), and dideprotonated (dianion, bta^{2-}) types (Scheme 1).

Moreover, H_2bta can be utilized as new bridging ligand for controlling the molecular architectures which, in combination with appropriate outer- and inner-sphere ligands, allows the variation of physicochemical and explosive properties within a wide range. H_2bta and its deprotonated modes might serve as a ligand in new generation of high-performance energetic materials with increased safety, as compared to-azide based PC's, in which the azide group is hidden in a aminotetrazole moiety, known to be stabilized by the extended 6π system.[9]

In this contribution, we present our results on the reaction of Cu^{2+} ions in aqueous ammonia solution with H_2bta, yielding $Cu(bta)(NH_3)_2$ (**1**), $Cu(bta)(NH_3)_2 \cdot H_2O$ (**2**), and $(NH_4)_2Cu(bta)_2 * 2.5H_2O$ (**3**), depending on the reaction conditions. The crystal structures of **1** and **2** are discussed with respect to the coordination mode of bta^{2-}, which mediates, in the case of **1** and **2**, superexchange interactions between the adjacent magnetic transition-metal Cu^{II} cations. This antiferromagnetic interaction results from 1D copper chains over an hidden azide end-to-end bridge. Interestingly, the structural arrangement of **1** is completely changed by the presence of crystal-bound water in **2**. Azide-containing clusters and networks showing, depending on the bridging mode, a diverse array of magnetic properties (e.g., symmetric double-end-on azide bridges typically mediate strong ferromagnetic exchange, whereas symmetric end-to-end bridges mediate strong antiferromagentic-exchange interactions).[10] Moreover, some physicochemical properties (e.g., heat of formation, friction and impact sensitivity, and DSC) of the investigated compound with respect to high-energetic materials are discussed.

Experimental Section

Caution: H_2bta in its dehydrated form shows increased friction and impact sensitivity. Although the copper salts of bta are kinetically stable compounds and turned out to be insensitive to friction and impact, they are nonetheless energetic materials and appropriate safety precautions should be taken, especially when these compounds are prepared on a larger scale. Laboratories and personnel should be properly grounded and safety equipment such as Kevlar gloves, leather coat, face shield, and ear plugs are necessary, especially when manipulating bta salts in the dehydrated form.

Synthesis. All chemical reagents and solvents of analytical grade were obtained from Sigma-Aldrich Fine chemicals Inc. and used as supplied. Infrared (IR) spectra were recorded on a Perkin-Elmer Spektrum One FT-IR instrument as KBr pellets at 20 °C. C, H, and N determinations were performed with a Netsch Simultanous Thermal Analyzer STA 429.

[$H_2bta \cdot H_2O$]. Method 1. 2 M HCl (150 mL) was added to a 500 mL three-neck reaction flask containing a refluxing suspension of sodium dicyanamide (8.9 g, 0.1 mol), sodium azide (13.0 g, 0.2 mol), ethanol (80 mL), and water (50 mL) over a period of 4 h. The reaction mixture was allowed to reflux for a further 48 h. After the mixture was cooled to room temperature (RT), 20 mL of concentrated HCl was added, and the white precipitate was filtered off. The crude material was recrystallized from boiling water to give 15.22 g (89% yield) of white amorphous **30**.

Method 2.[11] Pulverized cyanogen bromide (10.59 g, 0.1 mol) was added in small portions at 0 °C to a solution of aminotetrazole monohydrate (10.31 g, 0.1 mol) and sodium hydroxide (4.00 g, 0.1 mol) in 40 mL of water and 25 mL of EtOH. After the solution was stirred for 2 h at 0 °C and 3 h at RT, sodium azide (6.50 g, 0.1 mol) was added. Over a period of 3 h, 75 mL of 2M HCl was added to the refluxing mixture, and refluxing was continued for further 48 h. The product (13.5 g, 79% yield) was obtained according to the workup procedure outlined in Method 1. mp: 263 °C (dec). IR (KBr, cm^{-1}): ν 3456 (s), 3028 (s), 2932 (s), 2858 (s), 2671 (m), 2438 (m), 1796 (w), 1656 (vs), 1611 (s), 1556 (s), 1454 (m), 1352 (m), 1337 (m), 1282 (m), 1263 (m), 1154 (w), 1110 (m), 1072 (s), 1501 (s), 1036 (m), 1003 (m), 899 (m, br), 819 (m), 790 (m), 738 (m), 690 (m), 503 (m, br), 406 (w). Raman (200 mW, 25 °C, cm^{-1}): ν 3328 (11), 3120 (8, br), 1649 (9), 1618 (34), 1552 (54), 1480 (22), 1455 (17), 1370 (17), 1346 (15), 1267 (25), 1226 (26), 1151 (15), 1128 (15), 1073 (100), 1039 (42), 838 (7), 794 (17), 736 (9), 670 (7), 421 (22), 409 (48), 381 (9), 348 (20), 321

(7) Norris, W. P.; Henry, R. A. *J. Am. Chem. Soc.* **1963**, *29*, 650.
(8) (a) Hiskey, M. A.; Chavez, D. E.; Naud, D. L. U.S. Patent 6,214,39, 2001. (b) Hiskey, M. A.; Chavez, D. E.; Naud, D. L. U.S. Patent 6,-458,227, 2003.
(9) Norris, W. P.; Henry, R. A. *J. Org. Chem.* **1964**, *29*, 650. (b) Atwood, J. L.; Smith, K. D. *J. Am. Chem. Soc.* **1973**, *95*, 1488.
(10) Woodward, J. D.; Backov, R. V.; Abboud, K. A.; Dai, D.; Koo, H.-J.; Whangbo, M.-H.; Meisel, M. W.; Talham, D. R. *Inorg. Chem.* **2005**, *44*, 638.
(11) Klapötke, T. M.; Kuffer, C.; Mayer, P.; Polborn, K.; Schulz, A.; Weigand, J. J. *Inorg. Chem.* **2005**, *44*, 5949.

(48), 172 (100), 147 (46). ^{1}H NMR (DMSO-d_6, 25 °C): δ 5.94 (s, br). ^{13}C NMR (DMSO-d_6, 25 °C): δ 154.7 (C). ^{15}N NMR (DMSO-d_6, 25 °C): δ −17.9 (N2), −123.8 (N1), −315.7 (NH). Anal. Calcd for $C_2H_5N_9O$ (100.08): C, 14.04; H, 2.95; N, 73.67. Found: C, 14.10; H, 2.62; N, 73.42.

[Cu(bta)(NH$_3$)$_2$], 1. Single crystals suitable for X-ray analysis were obtained as follows. A solution of $CuCl_2 \cdot 2H_2O$ (170.5 mg, 1 mol) in 5 mL of water was slowly added to a hot solution (70 °C) containing BTA·H_2O (342 mg, 2 mmol), 2.5 mL of concentrated NH_3, and 60 mL of water, producing a dark green solution. From this solution (kept in a 500 mL beaker), blue rodlike single crystals, suitable for structural determination, were grown within 2 days. The reaction can be smoothly scaled up to 100 mmol, giving **1** in a 95% yield as light blue precipitate. After crystallization, the product was collected and washed with EtOH. mp: 185−187 °C. IR (KBr, cm^{-1}): ν 3375 (m), 3325 (s), 3255 (m), 3134 (m), 3057 (m), 2919 (m), 2826 (m), 1627 (vs), 1546 (s), 1499 (s), 1464 (m), 1446 (m), 1327 (m), 1235 (s), 1160 (w), 1140 (w), 1123 (m), 1116 (m), 1093 (w), 1083 (w), 1017 (w), 853 (vw), 808 (w), 747 (s), 727 (s), 678 (m), 620 (w), 440 (vw), 416 (w). Anal. Calcd for $CuC_2H_7N_{11}$ (248.70): C, 9.66; H, 2.84; N, 61.95. Found: C, 9.82; H, 2.91; N, 61.66.

[Cu(bta)(NH$_3$)$_2$·H$_2$O], 2. Single crystals suitable for X-ray analysis were obtained as follows. A solution of $CuCl_2 \cdot 2H_2O$ (341 mg, 2 mol) in 10 mL of water was slowly added to a refluxing solution containing BTA·H_2O (684 mg, 4 mmol), 20 mL of concentrated NH_3, and 10 mL of water, producing a deep blue solution. After a few minutes, compound **1** started to precipitate from this solution. The mixture was refluxed for a further 10 min, and the precipitate was filtered off. The filtrate was kept in a closed flask, from which, in approximately 3 weeks, compound **2** crystallized as big dark-blue octahedral crystals (yield 15%). Compound **2**, stored on air, slowly loses the crystal-bound water. IR (KBr, cm^{-1}). Anal. Calcd for $CuC_2H_9N_{11}O$ (266.71): C, 9.01; H, 3.41; N, 57.77. Found: C, 9.12; H, 3.38; N, 57.68.

[(NH$_4$)$_2$Cu(bta)$_2$·2.5H$_2$O], 3. A solution of $CuCl_2 \cdot 2H_2O$ (1.705 g, 10 mol) in 15 mL of water was slowly added to a hot solution (70 °C) containing BTA·H_2O (3.420 g, 20 mmol), 10 mL of concentrated NH_3, and 50 mL of water, producing a dark black-green solution. This solution was stirred for an additional 30 min at 70 °C. After the solution was cooled, very fine blue-black needles of **3** crystallized and were collected and washed with EtOH (yield 84%). mp: >250 °C (dec). IR (KBr, cm^{-1}): ν 3415 (s), 3313 (m), 3159 (m), 3034 (s), 2921 (s), 2807 (m), 1635 (s, shoulder), 1626 (vs), 1548 (s), 1502 (m), 1439 (vs, br), 1329 (m), 1257 (m), 1168 (w), 1124 (m), 1088 (w), 806 (m), 746 (m), 688 (m). Anal. Calcd for $CuC_4H_{15}N_{20}O_{2.5}$ (446.84): C, 10.75; H, 3.38; N, 62.69. Found: C, 11.00; H, 3.20; N, 62.81.

X-ray Structure Determination. Crystals were obtained as described above. The X-ray crystallographic data for **1** (CCDC 269320) were collected at 200 K on a STOE IPDS area detector, and for **2** (CCDC 269321), the data were collected at 213 K on SIEMENS P4 diffractometer equipped with a Siemens CCD area detector using graphite-monochromated Mo Kα radiation (λ = 0.71073 Å). The structures were solved by direct methods (SIR97 (**1**) and SHELXS-90 (**2**))[12] and refined by means of full-matrix least-squares procedures using SHELXL-97. For **2**, numerical absorption correction was performed using SADABS, and for **1**, XRed was used.[13] Crystallographic data are summarized in Table 1. Selected bond lengths and angles are available in Table 2. All non-hydrogen atoms were refined anisotropically. The hydrogen atoms of compounds **1** and **2** were located from the difference electron-density map and refined isotropically.

Table 1. Crystal Data and Details of the Structural Determination for Compounds **1** and **2**

	1	**2**
formula	$CuC_2H_7N_{11}$	$CuC_2H_9N_{11}O$
fw (g mol^{-1})	248.70	266.74
cryst syst	monoclinic	monoclinic
space group	$P2_1/n$	$P2_1/c$
a (Å)	6.3778(5)	7.596(2)
b (Å)	9.1886(7)	13.056(3)
c (Å)	14.2064(9)	9.170(2)
β (deg)	93.633(8)	94.20(3)
V (Å^3)	830.9(1)	907.0(3)
Z	4	4
ρ_{calcd} (g/cm^{-3})	1.9882(2)	1.953
μ (mm^{-1})	2.611	2.407
λ(Mo Kα) (Å)	0.71073	0.71073
T (K)	200(2)	213
reflns collected	6667	4087
independent reflns	1992	1741
R_{int}	0.0395	0.0234
observed reflns	1595	1557
F(000)	500	540
R1[a]	0.0241	0.0250
wR2[b]	0.0561	0.0686
weighting scheme[c]	0.0339, 0.000	0.0430, 0.5164
GOF	0.952	1.025
no. params	155	172
CCDC	269320	269321

[a] $R1 = \sum||F_0| - |F_c||/\sum |F_0|$. [b] $wR2 = [\sum(F_0^2 - F_c^2)/\sum w(F_0)^2]^{1/2}$. [c] $w = [\sigma_c^2(F_0^2) + (xP)^2 + yP]^{-1}$, $P = (F_0^2 - 2F_c^2)/3$.

Table 2. Selected Geometric Parameters (Å, deg) of **1** and **2**[a]

	1	**2**		**1**	**2**
N5−C1	1.362(3)	1.376(3)	N1−N2	1.353(2)	1.363(3)
N5−C2	1.369(3)	1.375(3)	N8−N9	1.359(3)	1.364(2)
C1−N1	1.345(2)	1.334(3)	N2−N3	1.306(2)	1.296(3)
C2−N9	1.330(2)	1.337(3)	N7−N8	1.301(2)	1.301(3)
C1−N4	1.325(3)	1.324(3)	N3−N4	1.362(2)	1.360(3)
C2−N6	1.325(3)	1.329(3)	N6−N7	1.355(3)	1.363(3)
Cu−N1	1.999(2)	1.997(2)			
Cu−N9	1.977(2)	1.996(2)			
Cu−N10	2.005(2)	2.004(2)			
Cu−N11	2.007(2)	2.033(2)			
Cu−N3a	2.319(2)^{i}	2.269(2)^{i}			
N1−Cu−N9	85.55(7)	85.40(8)	N3−Cu−N10	87.01(7)^{i}	91.75(9)^{i}
N1−Cu−N10	91.70(7)	89.63(9)	N3−Cu−N11	99.85(8)^{i}	97.95(8)^{i}
N1−Cu−N11	154.83(9)	166.98(9)	Cu−N1−N2	125.2(1)	123.5(1)
N1−Cu−N3	105.20(7)^{i}	95.02(7)^{i}	Cu−N1−C1	129.7(1)	131.1(2)
N9−Cu−N10	176.74(8)	170.25(8)	Cu−N3−N2	119.3(1)^{ii}	121.2(2)^{ii}
N9−Cu−N11	91.32(8)	91.9(1)	Cu−N3−N4	127.4(1)^{ii}	126.7(1)^{ii}
N3−Cu−N9	92.01(7)^{i}	97.03(8)^{i}	Cu−N9−N8	124.5(1)	124.5(1)
N10−Cu−N11	91.91(8)	91.1(1)	Cu−N9−C2	129.9(2)	130.9(2)

[a] Symmetry codes for **1**: (i) $-0.5 - x$, $0.5 + y$, $0.5 - z$; (ii) $-0.5 - x$, $-0.5 + y$, $0.5 - z$. **2**: (i) x, $1.5 - y$, $0.5 + z$; (ii) x, $1.5 - y$, $-0.5 + z$.

Magnetic Measurements. Bulk magnetization measurements of pulverized samples were performed on a Quantum Design MPMSR-XL SQUID magnetometer in a temperature range from 2 to 300 K. All measurements were carried out at two field strengths (0.2 and 0.5 T). Diamagnetic corrections were made using estimated values according to $\chi_{dia} \approx -0.5 \times 10^{-6} M_{complex}$.

EPR Measurements. EPR investigations were carried out on a ESP 300E (Bruker) instrument at room temperature on the solid.

(12) (a) Altomare, A.; Burla, M. C. M.; Camalli, M.; Cascarano, G. L.; Giacovazzo, C.; Guagliardi, A.; Moliterni, A. G. G.; Polidori, G.; Spagna, R. *J. Appl. Crystallogr.* **1999**, *32*, 115−119. (b) Sheldrick, G. M. *SHELXL-90, Program for Solution of Crystal Structures*; University of Göttingen: Göttingen, Germany, 1990.

(13) (a) *SMART*, revision V4.C50; Brucker AXS INC.: Madison, WI. (b) *XRed*, revision 1.09; Darmstad, Germany.

DSC and TGA measurements. The differential scanning-calorimeter experiments for **1** and **3** were performed with an Perkin-Elmer Pyris 6 DSC, calibrated with standard pure indium and zinc. Measurements were performed at a heating rate of $\beta = 2$, 5, 10, and 15 °C in closed Al containers with a hole (1 μm) on the top for gas release with a nitrogen flow rate of 20 mL/min. The reference sample was an Al container with air. The energy of activation for the decomposition step was estimated by the method of Ozawa[14] by following the differential heating-rate method of the American Society for Testing and Materials (ASTM) according to ASTM protocol E 698-99.[15] The sample size was kept small to minimize temperature gradients within the sample and a 0.003*3/16 in. disk was used to optimize good thermal contact between the sample and container. Compounds **1** and **3** were subjected to TGA analysis in a nitrogen atmosphere in open Al_2O_3 crucibles (sample weight $\approx$ 5 mg) at a heating rate of 5 °C/min with a thermogravimetric analyzer (Setaram DTA-TGA 92) in the temperature range from 30 to 750 °C. All samples were dried in vacuo for 24 h at 40 °C to remove moisture.

Bomb Calorimetry. For all calorimetric measurements, a Parr 1356 bomb calorimeter (static jacket) equipped with a Parr 207A oxygen bomb for the combustion of highly energetic materials was used.[16] The samples (ca. 80−100 mg) were loaded in (energetically) calibrated Parr gelatine capsules (0.9 mL), and a Parr 45C10 alloy fuse wire was used for ignition. In all measurements, a correction of 2.3 (IT) calories per cm wire burned has been applied, and the bomb was examined for evidence of noncombusted carbon after each run. A Parr 1755 Printer was furnished with the Parr 1356 calorimeter to produce a permanent record of all activities within the calorimeter. The reported values are the average of three single measurements. The calorimeter was calibrated by combustion of certified benzoic acid (SRM, 39i, NIST) in an oxygen atmosphere at a pressure of 3.05 MPa. Typical experimental results of the constant-volume combustion energy ($\Delta_c U$) of the salts are summarized in Table 2. The standard molar enthalpy of combustion ($\Delta_c H°$) was derived from $\Delta_c H° = \Delta_c U + \Delta nRT$ ($\Delta n = \sum n_i$ (products, g) $- \sum n_i$ (reactants, g); $\sum n_i$ is the total molar amount of gases in the products or reactants). The enthalpy of formation, $\Delta_f H°$, for each of the corresponding salts were calculated at 298.15 K using designed Hess thermochemical cycles.

Results and Discussion

Compound Synthesis. The reaction of sodium dicyanamide with sodium azide under acid-catalyzed conditions yields the corresponding *N*,*N*-bis(1(2)*H*-tetrazol-5-yl)-amine as monohydrate ($H_2bta \cdot H_2O$).[17] This compound can easily be dehydrated under vacuum (24 h, 10^{-3} Torr) at elevated temperature (120 °C) yielding solvate-free *N*,*N*-bis(1(2)*H*-tetrazol-5-yl)-amine (H_2bta**)**. Compounds **1**, **2**, and **3** were synthesized by the direct combination of stoichiometric amounts (1:1, 1:1, and 1:2, respectively) of $CuCl_2 \cdot 2H_2O$ in water and $H_2bta \cdot H_2O$ in diluted ammonia solution (in the case of **2**, concentrated ammonia solution) under normal laboratory conditions. Compounds **1** and **3** can be easily synthesized in high batches within a short time and are obtained as light blue and black-blue precipitates, respectively. From diluted solution, compound **1** crystallizes as thin blue rods, suitable for X-ray structure determinations, within 2 days and compound **3** crystallizes as black-blue thin needles, which turned out to be unsuitable for structural determination. In the case of **2**, X-ray quality crystals were obtained from concentrated ammonia solution in an ammonia atmosphere within three weeks. In comparison to **1**, compound **2** crystallized as big deep-blue coarse crystals, octahedral in shape, which slowly loses, stored on air, the crystal-bound water.

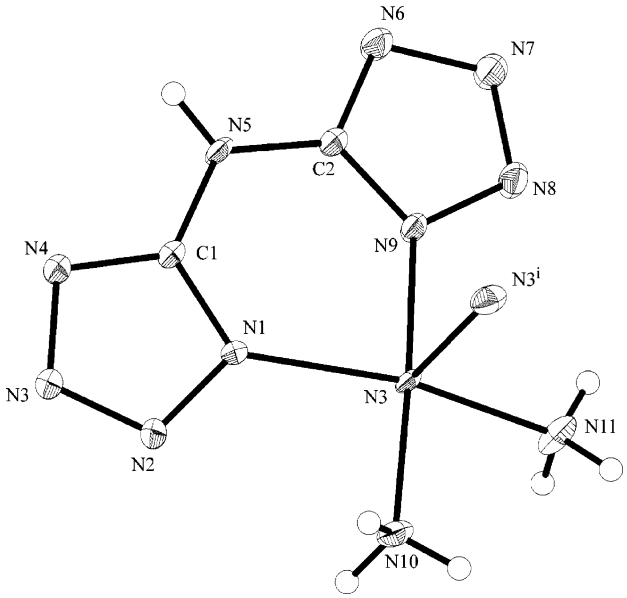

Figure 1. Coordination environment of the Cu^{II} ion in **1**, showing the atom numbering scheme. Displacement ellipsoids are drawn at the 50% probability level, and H atoms are shown as spheres of arbitrary radii. (symmetry code: (i) $-0.5 - x$, $0.5 + y$, $0.5 - z$).

Crystal Structures. Crystallographic and structural refinement data for compounds **1** and **2** are listed in Table 1, and selected bond length and angles are included in Table 2. Tables of atomic coordinates and thermal displacement parameters and a complete list of bond angles and distances for **1** and **2** can be obtained from the corresponding cif files in the Supporting Information. Only one labeled diagram is shown (Figure 1, (**1**)) as the molecular arrangement of **2** is similar. In the molecules of **1** and **2**, each Cu^{II} ion is five-coordinate, with a distorted square-pyramidal geometry. The basal plane is formed by atoms N1 and N9 from one bidentate bta ligand, along with atoms N10 and N11 from the two coordinated ammonia molecules, with a mean deviation of 0.2256 (**1**) and 0.0459 Å (**2**), respectively. The distortion from the square-pyramidal geometry is more pronounced in the case of **1** compared to that in **2**. With respect to the plane, in both cases, atoms N1 and N11 lie below and N9 and N10 lie above. A nitrogen molecule ($N3^i$) occupies the apical position (symmetry code: (**1**) (i) $-0.5 - x$, $0.5 + y$, $0.5 - z$; (**2**) (i) x, $1.5 - y$, $0.5 + z$) with a rather long distance observed for **1** (2.319(2) Å) in contrast to that for **2** (2.269(2) Å).

(14) Ozawa, T. *Bull. Chem. Soc. Jpn.* **1965**, *38*, 1881.
(15) Standard Test Methods for Arrhenius Kinetic Constants for Thermally Unstable Materials, ASTM designation E698−99, 1999.
(16) http://www.parrinst.com/.
(17) (a) Highsmith, T. K.; Hajik, R. M.; Wardle, R. M.; Blau, G. K.; Blau, R. J. U.S. Patent 5,468,866, 1995. (b) Naud, D. L.; Hiskey, M. A. U.S. Patent Application Publ. 2003060634; *Chem. Abstr.* **2003**, *138*, 255236. (c) Kita, M.; Ueda, T. Jpn. Kokai Tokkyo Koho JP 2004067544; *Chem. Abstr.* **2004**, *140*, 217643.

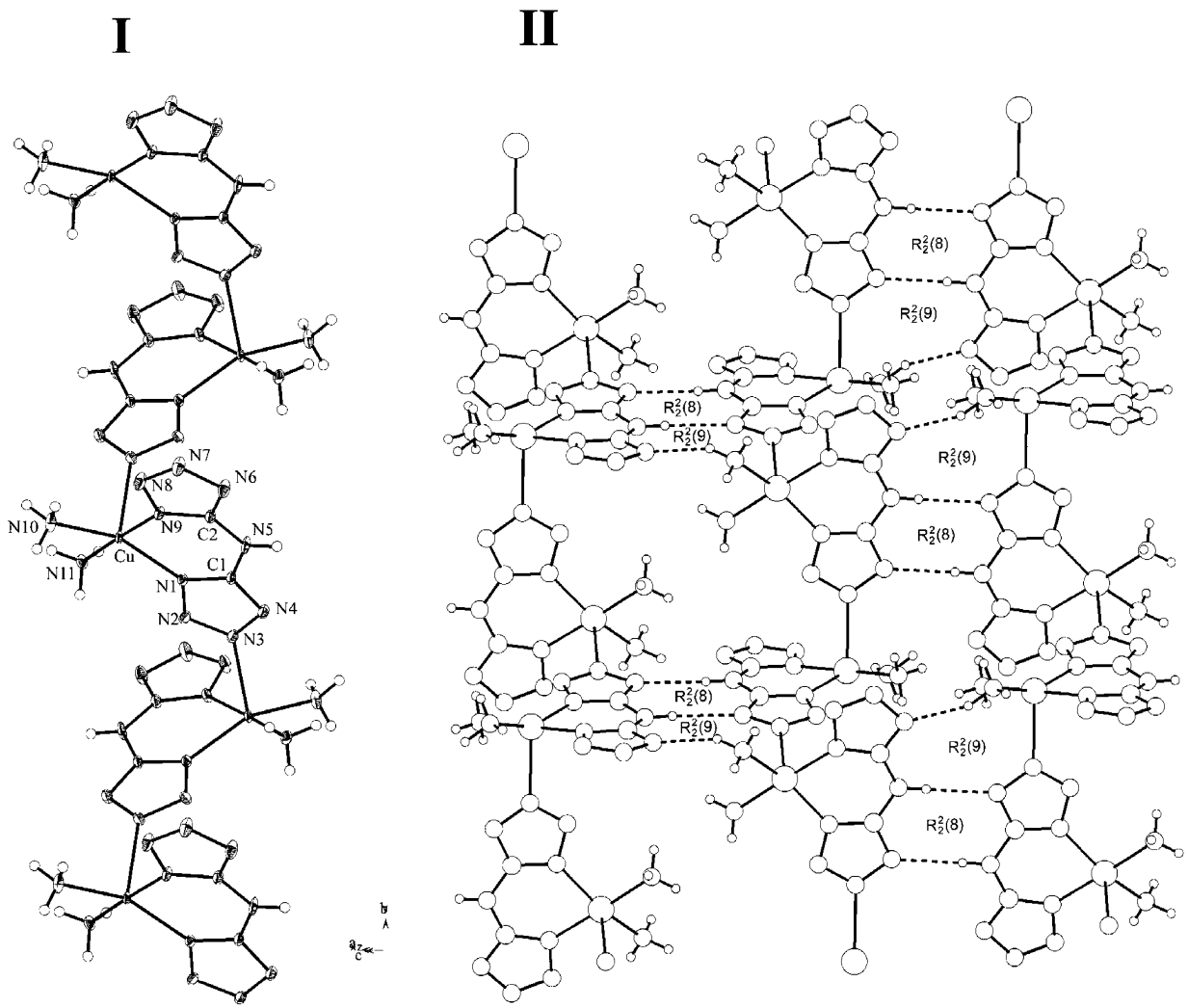

Figure 2. Crystal structure of **1**. **I**: Chains along the *b* axis; ORTEP plot drawn at the 50% probability level. **II**: Perspective view of the chains connected through hydrogen bonds to a pleated sheet.

The Cu−N bond length to the nitrogen atoms of the bta ligand, ranging from 1.977(2) to 1.999(2) Å (Table 2), are slightly shorter than the Cu−N bond length to the coordinated ammonia molecules (2.004(2)−2.033(2) Å) and are similar to those observed in comparable copper complexes with, for example, tertrazole or ammonia ligands.[18] The copper atom is not in the basal plane, but it is located 0.2064 (**1**) and 0.1884 (**2**) Å out of the mean basal plane toward N3^{i}. According to the valence-bond theory, if a Cu (d^9) ion is five-coordinate, there will be two probable coordination geometries around the metal ion (viz., trigonal-bipyramidal and square-pyramidal). In the former, the Cu ion adopts dsp^3 or sp^3d hybridization and in the latter d^2sp^2 or sp^2d^2. These two configurations of a d^9 ion possess approximately equal energy, and they can interconvert. The angular structural index parameter, τ, of the coordination polyhedron for the Cu^{II} ions in **1** and **2** has been calculated according Addison et al.[19] The distortion value, τ, accounts, in the case of **1**, for 0.365 and, in the case of **2**, for 0.0545. The τ value for both cases indicate that the coordination geometry around each Cu^{II} ion in **1** and **2** is a distorted square pyramid, being less distorted for the latter, and that the Cu (d^9) ions probably adopt sp^2d^2 hybrid orbitals to accept electrons from the ligands. This may be favorable to the paramagnetism and stability of **1** and **2**.

The obvious deviation of the coordination around the Cu^{II} in **1** compared to that in **2** cannot be easily explained by the comparison of the molecular structures alone. A closer inspection of the crystal structure of **1** and **2** reveals a

(18) (a) Lyakhov, A. S.; Gaponik, P. N.; Degtyarik, M. M.; Ivashkevich, L. S. *Acta Cryst.* **2003**, *C59*, m204. (b) Mills, A. M.; Flinzner, K.; Stassen, A. F.; Haasnoot, J. G.; Spek, A. L. *Acta Cryst.* **2002**, *C58*, m243; (c) Ivashkevich, L. S.; Lyakhov, A. S.; Gaponik, P. N.; Bogatikov, A. N.; Govorova, A. A. *Acta Cryst.* **2001**, *E57*, m335. (d) Gökaugac, G.; Tatar, L.; Kisakürek, D.; Ülkü, D. *Acta Cryst.* **1999**, *C55*, 1413. (e) Tatar, L.; Gökagac, G.; Ülkü, D. *Acta Cryst.* **2000**, *E56*, m335.

(19) (a) Addison, A. W.; Rao, T. N.; Reedijk, J.; van Rijn, J. *J. Chem. Soc., Dalton Trans.* **1984**, 1349. (b) The largest bond angles around the Cu(II) center (β: N(9)−Cu−N(10) = 176.74(8)° (**1**) vs N(9)−Cu−N(10) = 170.25(8)° (**2**)) are larger than the second-largest one (α: N(1)−Cu−N(11) = 154.82(7)° (**1**) vs N(1)−Cu−N(11) = 166.98-(8)° (**2**)). The value of the differences between the longest and shortest Cu−N bond distances of the basal atoms applied for ΔCu−N is 0.030 Å (**1**) and 0.036 Å (**2**), respectively. Since the angular structural index parameter, $\tau = (\beta - \alpha)/60$, is evaluated by the two largest angles ($\alpha < \beta$) in the five-coordinate geometry, the value of τ indicates a regular square-based pyramidal stereochemistry ($\tau = 1.0$) or a regular trigonal bipyramidal stereochemistry ($\tau = 0.0$).

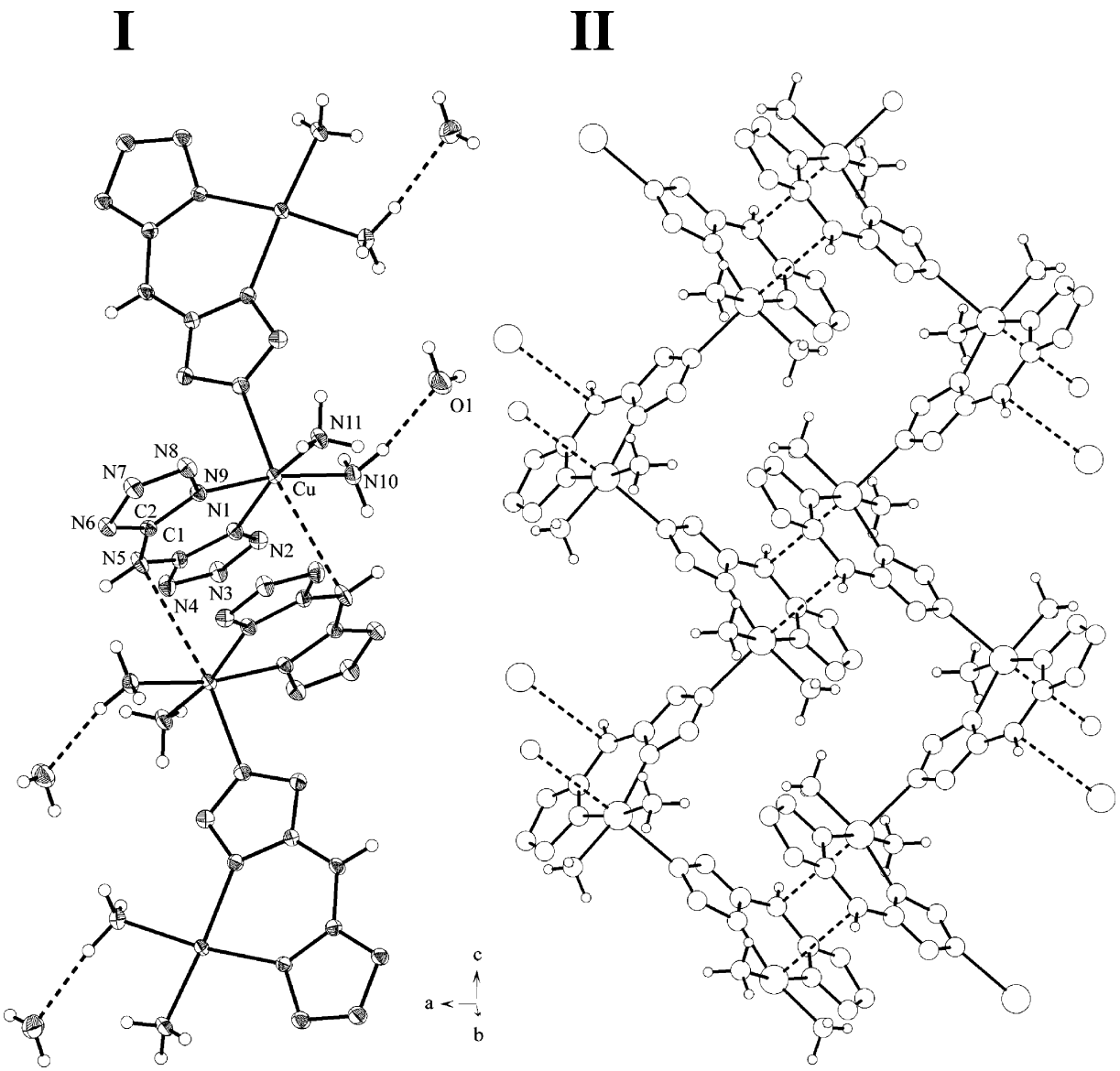

Figure 3. Crystal structure of **2**. **I**: Chains along the *c* axis; ORTEP plot drawn at the 50% probability level. **II**: Perspective view of the chains connected through interlocking.

completely different picture of the molecular arrangements. In both complexes, each bta dianion acts as a tridentate ligand toward copper, connecting two Cu^{II} ions trough the N1, N9, and N3 nitrogen atoms, resulting in a one-dimensional zigzag chain. The Cu···Cu^{i} separation was found to be 6.1350(3) Å in **1** (Figure 2) and 6.116(1) Å in **2** (Figure 3) (symmetry code: (**1**) (i) $-0.5 - x$, $0.5 + y$, $0.5 - z$; (**2**) (i) x, $1.5 - y$, $0.5 + z$). The folded chains in **1** are orientated in a one-dimensional zigzag pattern along [010]. These chains, orientated in an antiparallel manner, are linked over two strong hydrogen bonds (N10−H1···$N7^{ii}$ and N5−H7···$N4^{v}$ (symmetry code: (ii) $-0.5 + x$, $0.5 - y$, $0.5 + z$; (v) $-1 - x$, $-y$, $-z$) to a pleated sheet (Figure 2, **II**). The most important hydrogen bonded ring motif of this sheet, in the formalism of the graph-set analysis of the hydrogen-bond patterns,[20] is identified as $R_2^2(9)$ and the very common $R_2^2(8)$. The sheetlike structure in **1** is reminiscent of the β-pleated sheet structure of proteins. The pleated sheets are connected to a 3D network by further hydrogen bonds (Table 3).

In contrast to **1**, the arrangement of the molecules in the crystal structure of **2** is different. Although **2** forms folded chains which are orientated in a one-dimensional zigzag pattern along [001], these chains are not connected through hydrogen bonds to a pleated sheet. Rather, they interlock with each other, forming herringbone-type sheets. The smallest subunit of two interlocking chains is depicted in Figure 3 (**I**).

If at all, this interaction between such a dimeric unit might result from a electrostatic interaction because the distance between the Cu^{II}−$N3^{iii}$ of 3.285(3) (symmetry code: (iii) $2 - x$, $2 - y$, $1 - z$) is much longer than the sum of the van der Waals radii ($r_{A(Cu)} + r_{D(N)} = 2.95$ Å),[21] and therefore should be related to packing effects. One chain related to the next is counter-rotated with respect to the running

(20) (a) Etter, M. C. *Acc. Chem. Res.* **1990**, *23*, 120. (b) Etter, M. C.; MacDonald, J. C. *Acta Crystallogr.* **1990**, *B46*, 256.

(21) Bondi, A. *J. Phys. Chem.* **1964**, *68*, 441.

Table 3. Hydrogen Bond Geometry (Å, deg) of **1** and **2**[a]

D−H···A	D−H	H···A	D···A	D−H···A
		1		
N10−H1···N7^{ii}	0.91(3)	2.30(3)	3.194(3)	167(2)
N10−H2···N8^{iii}	0.84(4)	2.33(3)	3.043(3)	142(3)
N11−H4···N8^{b}	0.78(4)	2.45(3)	2.982(3)	127(3)
N11−H5···N6^{iv}	0.92(4)	2.06(4)	2.927(3)	155(3)
N5−H7···N4^{v}	0.83(3)	2.14(3)	2.966(2)	177(2)
		2		
N10−H1···N7^{ii}	0.88(3)	2.35(3)	3.191(3)	159(3)
N11−H4···N8^{iii}	0.90(4)	2.31(4)	3.203(3)	169(3)
N11−H5···N8^{b}	0.77(4)	2.52(4)	3.003(4)	122(3)
N5−H7···N6^{iv}	0.89(3)	2.05(3)	2.929(3)	172(2)
N10−H3···O1	0.92(4)	2.03(4)	2.939(3)	170(3)
O1−H1A···N4^{v}	0.71(4)	2.28(4)	2.970(3)	166(5)
O1−H1B···N7^{iii}	0.83(4)	2.21(4)	3.015(3)	163(3)

[a] Symmetry codes for **1**: (i) $-0.5 - x$, $0.5 + y$, $0.5 - z$; (ii) $-0.5 + x$, $0.5 - y$, $0.5 + z$; (iii) $0.5 - x$, $-0.5 + y$, $0.5 - z$; (iv) $0.5 + x$, $0.5 - y$, $0.5 + z$; (v) $-1 - x$, $-y$, $-z$. **2**: (i) x, $1.5 - y$, $0.5 + z$; (ii) $2 - x$, $-0.5 + y$, $0.5 - z$; (iii) $2 - x$, $2 - y$, $1 - z$; (iv) $3 - x$, $2 - y$, $-z$; (v) $1 + x$, $1.5 - y$, $0.5 + z$. [b] Intramolecular hydrogen bond

direction. The resulting herringbone-type sheets are connected through the water molecule, the ammonia, and the NH group to a 3D network (Table 3). Again, hydrogen bond N5−H7···N6^{iv} (symmetry code: (iv) $3 - x$, $2 - y$, $-z$] results in the occurrence of the well-known $R_2^2(8)$ graph set (not depicted in Figure 3), yet resulting from the interaction of the layers compared to **2**. In the case of **3**, a complete structural solution could not be performed because of the unsolvable disorder of the crystal-bound water molecules, therefore we abstain from a detailed discussion of the crystal structure (Supporting Information Figure S1).

Magnetism and Coordination Structures. The magnetic susceptibility of the three complexes has been measured in the temperature range of 300−2 K. The temperature dependence of $\chi_M T$ is shown in Figure 4 for compound **1** and **2** and in Figure 5 for compound **3**. The $\chi_M T$ product at room temperature is 0.47 (**1**), 0.52 (**2**), and 0.43 cm^3 K mol^{-1} (**3**) larger than the spin-only value of 0.37 expected for a single copper(II) ion ($S = 1/2$), assuming $g = 2.00$. When cooled, $\chi_M T$ decreases significantly for compounds **1** and **2**, while the product is nearly constant in the case of compound **3**. The magnetic behavior of compound **1** and **2** is characteristic for antiferromagnetically coupled copper centers. To estimate the magnitude of the antiferromagnetic coupling, the magnetic data were fitted using the equation for equally spaced copper(II) ions first applied by Bonner and Fisher[22] with the Hamiltonian in the form

$$H = -J \sum_{i=1}^{n-1} S_{Ai} S_{Ai+1}.$$

The magnetic data of all three complexes were fitted leading to the parameters $J = -7.82 \pm 0.30$ cm^{-1}, $g = 2.26 \pm 0.01$ (compound **1**); $J = -5.95 \pm 0.13$ cm^{-1}, $g = 2.39 \pm 0.01$ (compound **2**); and $J = -0.38 \pm 0.03$ cm^{-1}, $g = 2.11 \pm 0.01$ (compound **3**). The antiferromagnetic coupling is rather weak in all three cases, especially for compound **3**, where the distance to the apical nitrogen atom is rather long. The reason for the weak interaction is that the magnetic orbitals, describing the single electron on the copper centers are mainly of the $d_{x^2-y^2}$ type. The bta dianion connecting the copper centers through the N1, N9, and N3 nitrogen atoms belong to the basal plane of Cu (N1 and N9) but occupies an axial position in the square-pyramidal coordination sphere on the neighboring Cu (N3). Consequently, the interactions between the magnetic orbitals of the two copper centers are very weak leading to small coupling parameters. Similar

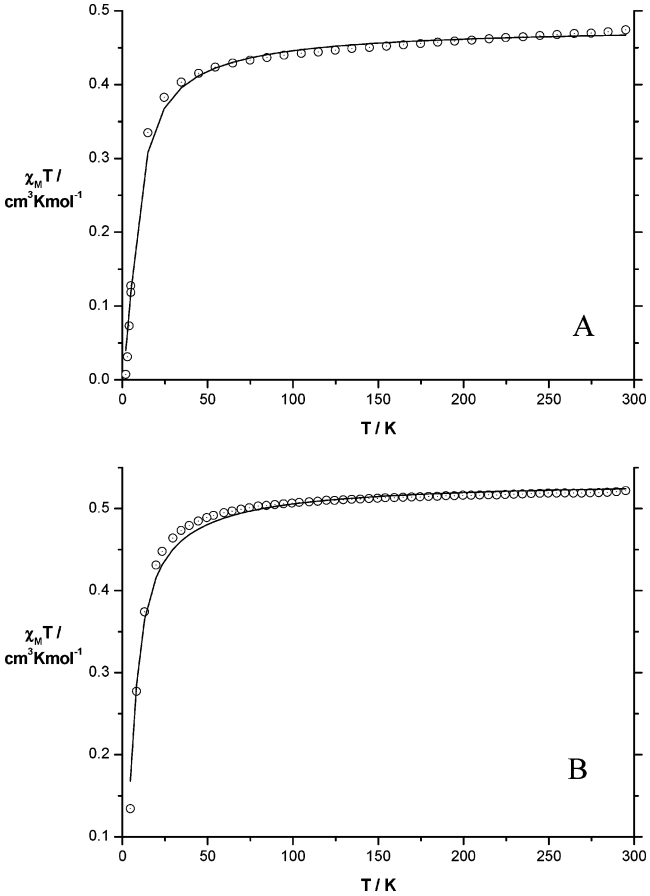

Figure 4. Plot of $\chi_M T$ vs T for **1** (A) and **2** (B) under an applied magnetic field of 0.5 T. Solid lines represent the best fit of the date with the model described in the text.

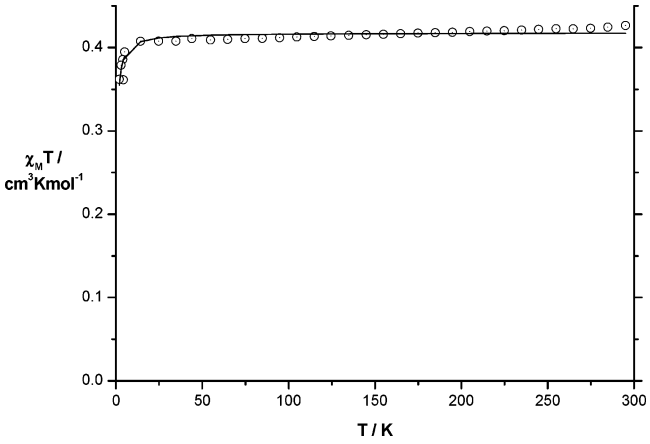

Figure 5. Plot of $\chi_M T$ vs T for **3** under an applied magnetic field of 0.5 T. Solid lines represent the best fit of the date with the model described in the text.

(22) (a) Kahn, O. *Molecular Magnetism*; VCH: New York, 1993. (b) Bonner, J. C.; Fisher, M. E. *Phys. Rev.* **1964**, *135*, 640.

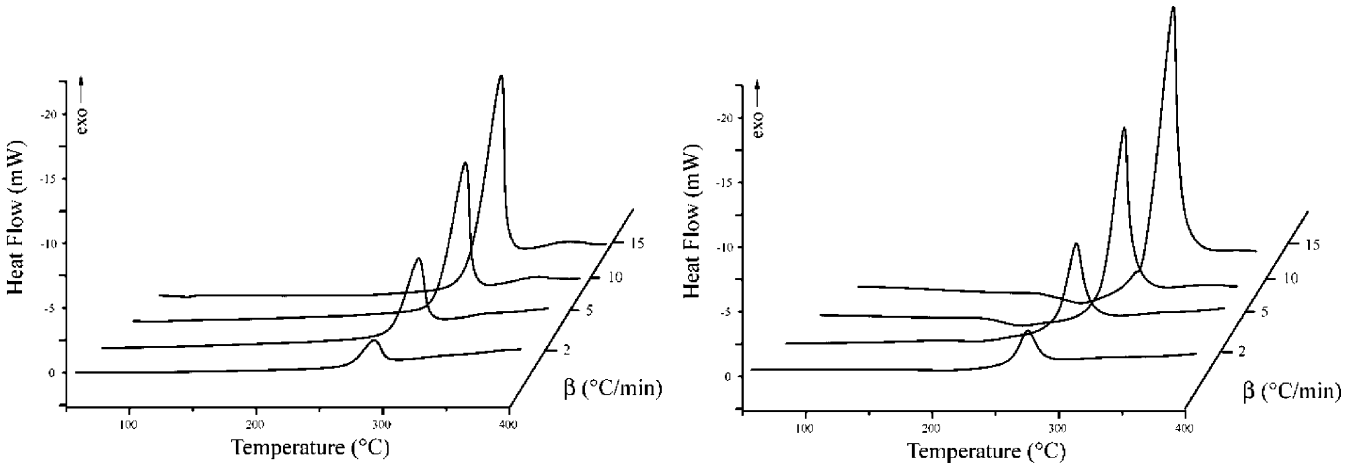

Figure 6. DSC thermographs of **1** (left) and **2** (right) (β = 2, 5, 10, and 20 °C/min).

observations were made for end-on azido-bridged copper complexes[23] and oxalato-bridged systems.[24] An explanation for the small differences in the coupling parameters of compound **1** and **2** cannot be found in the molecular structure of the two complexes.

The differences in the coordination environment of the copper centers are also reflected in the powder X-Band EPR spectra. Compounds **1** and **2**, with the square-pyramidal coordination environment, exhibit spectra with a rhombic symmetry and clearly separated g tensor ($g_1 = 2.184$, $g_2 = 2.094$, and $g_3 = 2.045$; $g_{iso} = 2.108$ for compound **1**). In complex **3**, with very long apical Cu−N distances and local symmetry close to that of a distorted tetrahedron, a spectrum of a cubic system with a small distortion ($g = 2.087$) is obtained. The fitted g values obtained from the magnetic measurements are slightly higher than the values measured.

Thermal Decomposition and Thermodynamic Aspects. The DSC thermograms of **1** and **3** for different heating rates (β = 2, 5, 10, and 15 °C/min) are presented in Figure 6. The decomposition, in the case of **1**, occurs in two steps between 250 and 400 °C, and the final residue, estimated to be copper, has an observed mass of 26.2% versus the calculated value of 25.5%. The second step can only be noticed as a weak exothermic effect between 300 and 400 °C in the DSC. Interestingly, the decomposition is comparable to that of an ammoniacal complex of copper oxalate and indicates that the first decomposition step might be determined as the deammoniation of **1**.[25] In the case of **3**, the decomposition also occurs in two steps, in which the first step corresponds to the loss of crystal-bound water. This process is not well resolved in the DSC because the release of water does not proceed stepwise. As indicated in the TGA experiment, the release of water occurs within a temperature range of 70−170 °C with a mass loss of 10.4% (Calcd: 10.0%). The second exotherm occurs in a sharp temperature range at 250−270 °C with a mass loss of 80.0% (Calcd: 75.8%).[26]

Table 4. Physicochemical Properties of **1** and **3**

	1	**3**
formula	$CuC_2H_7N_{11}$	$CuC_4H_{15}N_{20}O_{2.5}$
molar mass	248.70	446.84
N (%)	62.0	64.0
Ω (%)[a]	−48.3	−47.5
β (°C)		
2	284.00	266.65
5	295.80	275.14
10	305.11	282.60
15	310.46	287.31
T_{int}[b]	250−300; 300−400	70−150; 250−270
$\Delta_{max}H$ (cal/g)[c]	−103.8	−121.5 J/g
E_a (kcal mol^{-1})[d]	46.90 ± 0.16	56.46 ± 1.16
$-\Delta_C U_m$ (cal/g)[e]	2233.8	1989.3
$-\Delta_C H_m^\circ$ (kcal mol^{-1})[f]	555.5	862.7
$\Delta_f H_m^\circ$ (kcal mol^{-1})[g]	+87.8	−29.2
$-\Delta_E H_m^\circ$ (kcal/kg)[h]	398.2	236.5
density (g cm^{-3})	1.9882(2)	1.353[l]
impact (J)[i]	>40	>40
friction (N)[j]	>360 (−)	>360 (−)
gas volume (25°C) (ml/g)[k]	819	837

[a] Oxygen balance. [b] Range of decomposition by TGA (β = 5 °C). [c] Heat of combustion from maximum exothermic step (DSC). [d] Activation energy according Ozawa[14]. [e] Experimental constant volume combustion energy. [f] Experimental molar enthalpy of combustion. [g] Molar enthalpy of formation. [h] Calculated molar enthalpy of detonation, ICT thermodynamic code see ref 33. [i,j] Ref 29. [k] Assuming only gaseous products, ICT thermodynamic code see ref 33. [l] Estimated from a structure determination.

As can be seen from Table 4, as the heating rate increases, the temperature of the exothermic maxima also increases. The kinetics of exothermic reactions are important in assessing the potential of materials and systems for thermal explosion, and the activation energy for compound **3** (56.46 ± 0.16 kcal mol^{-1}) was estimated to be 9.5 kcal mol^{-1} higher than that of **1** (46.90 ± 0.16 kcal mol^{-1}), but it still indicates good thermal stability for both complexes. For initial safety testing, the impact and friction sensitivity was tested according to BAM methods with the "BAM Fallhammer"[27] and "BAM friction tester",[28] and both compounds are

(23) Koner, S.; Saha, S.; Mallah, T.; Okamoto, K.-I. *Inorg. Chem.* **2004**, *43*, 840.
(24) Julve, M.; Verdaguer, M.; Gleizes, A.; Philoche-Levisalles, M.; Kahn, O. *Inorg. Chem.* **1984**, *23*, 3808.
(25) Prasad, R. *Thermochim. Acta* **2003**, *406*, 99.

(26) This discrepancy might be explained by the strong explosion process of the compound during the second steps which leads to the loss of material in the crucible.
(27) Test methods according to the UN Recommendations on the Transport of Dangerous Goods, Manual of Tests and Criteria, fourth revised edition, United Nations Publication, New York and Geneva, **2003**, ISBN 92-1-139087-7, Sales No. E.03.VIII.2.; 13.4.2 Test 3(a)(ii) BAM Fallhammer.

insensitive toward impact (>40 J) and friction (>360 N) (Table 4).

The heats of combustion for dehydrated bta and compounds **1** and **3** were determined experimentally, and the values of the molar enthalpy of formation were calculated from a designed Hess thermochemical cycle according to reactions 1−3, and they are summarized in Table 4 for compounds **1** and **3**.

$$\mathbf{1}:\ CuC_2H_7N_{11}(s) + 6O_2 \rightarrow CuO(s) + 2CO_2(g) + 3.5H_2O(l) + 5.5N_2(g) \quad (1)$$

$$\mathbf{3}:\ CuC_4H_{14}N_{20}O_2(s) + 7O_2 \rightarrow CuO(s) + 4CO_2(g) + 7H_2O(l) + 10N_2(g) \quad (2)$$

$$\mathbf{BTA}:\ C_2H_3N_9(g) + 11/4O_2(g) \rightarrow 2CO_2(g) + 3/2H_2O(g) + 9/2N_2(g) \quad (3)$$

$$\Delta_f H^\circ_m = \Delta_f H^\circ_m(CuO,s) + x\Delta_f H^\circ_m(CO_2,g) + y\Delta_f H^\circ_m(H_2O,l) - \Delta_c H^\circ_m$$

The enthalpy criteria of energetic materials are governed by their molecular structure, and therefore, the move to heterocycles with a higher nitrogen content (e.g., from imidazole ($\Delta_f H^\circ_{cryst}$ = 14.0 kcal mol^{-1})[30] to 1,2,4-triazole ($\Delta_f H^\circ_{cryst}$ = 26.1 kcal mol^{-1}) to tetrazole ($\Delta_f H^\circ_{cryst}$ = 56.7 kcal mol^{-1})[31]) the trend in the values of the heat of formation is obvious. Therefore, bta^{2-} as ligand also should lead to increased values for the heat of formation. The heat of combustion of dehydrated bta (eq 3) was determined experimentally from five independent measurements to be $\Delta_c H_m = -418.5 \pm 9$ kcal mol^{-1}. With the experimentally determined enthalpy of combustion and the known enthalpies of formation (0 kcal mol^{-1}), CO_2 (−94.2 kcal mol^{-1}), H_2O (−68.1 kcal mol^{-1}), and N_2 (0 kcal mol^{-1}),[32] the heat of formation of dehydrated bta was calculated to be $\Delta_f H^\circ_m(H_2bta) = +128.0$ kcal mol^{-1}.

From the values obtained for the heat of formation and the densities obtained from the crystal structure determinations, some thermochemical properties have been calculated using the ICT thermodynamic code and are depicted in Table 4.[33]

Conclusion

Depending on the reaction conditions, $Cu(bta)(NH_3)_2$ (**1**), $Cu(bta)(NH_3)_2 \cdot H_2O$ (**2**), and $(NH_4)_2Cu(bta)_2 \cdot 2.5H_2O$ (**3**) could be synthesized. In the case of **1** and **3**, a scale-up procedure is possible because **1** and **2** are easily accessibly from cheap starting materials and riskless to handle. Complexes **1** and **3** are certainly of interest as additives in *pyrotechnics*, AP-based *propellants*, or other applications, as they show promising properties with respect to stability, sensitivity, and energetic aspects. Furthermore, the crystal structures of **1** and **2** were discussed with respect to the coordination mode of bta^{2-}, which mediates, in the case of **1** and **2**, weak superexchange interactions between the adjacent magnetic transition-metal Cu^{II} cations, resulting from 1D copper chains over an hidden azide end-to-end bridge. The structural arrangement of **1** completely changes from a pleated layerlike structure reminiscent of the β-pleated sheet structure of proteins to herringbone-type sheets in the case of **2**. These structural features have been discussed with respect of the occurrence of well-known graph sets. It makes sense to compare azide-containing clusters and networks with the bta ligand since bta can be regarded as hidden azide. Depending on the bridging mode of the azide in such clusters and networks, a diverse array of magnetic properties is observed (e.g., symmetric double-end-on azide bridges typically mediate strong ferromagnetic exchange, whereas symmetric end-to-end bridges mediate antiferromagentic-exchange interactions). The latter counts exactly for the bta^{2-} ligand, as shown by the magnetic measurements performed on the investigated complexes.

Acknowledgment. The authors are indebted to and would like to thank Prof. Dr. P. Klüfers and Prof. Dr. H. Nöth for their generous allocation of X-ray diffractometer time. Financial support of this work by the University of Munich (LMU) and the Fonds der Chemischen Industrie is gratefully acknowledged. J.J.W. is grateful for a FCI PhD fellowship (DO 171/46) and an Alexander von Humboldt postdoctoral scholarship. The authors are also indebted to and would like to thank Gunnar Spiess for the caloric measurements and the sensitivity tests.

Supporting Information Available: Crystallographic details for compound **3**. This material is available free of charge via the Internet at http://pubs.acs.org. Further information on the crystal-structure determinations (excluding structure factors) has been deposited with the Cambridge Crystallographic Data Centre as supplementary publication Nos. 269320 and 269321. Copies of the data can be obtained free of charge by application to CCDC, 12 Union Road, Cambridge CB2 1EZ, UK (fax, (+44) 1223−336−033; e-mail, deposit@ccdc.cam.ac.uk).

IC050657R

(28) Reichel & Partner GmbH, http://www.reichel-partner.de/.

(29) [i] Insensitive > 40 J, less sensitive ≥ 35 J, sensitive ≥ 4, very sensitive ≤ 3 J; [j] Insensitive > 360 N, less sensitive = 360 N, sensitive < 360 N a. > 80 N, very sensitive ≤ 80 N, extreme sensitive ≤ 10 N.; According to the UN Recommendations on the Transport of Dangerous Goods (+) indicates not safe for transport.

(30) West, R. C.; Selby, S. M. *Handbook of Chemistry and Physics*, 48th ed.; The Chemical Rubber Co.: Cleveland, OH, 1967−1968; pp D22−D51.

(31) Ostrovskii, V. A.; Pevzner, M. S.; Kofman, T. P.; Tselinskii, I. V. *Targets Heterocycl. Syst.* **1999**, *3*, 467−526.

(32) *NIST Chemistry WebBook*, NIST Standard Reference Database Number 69; March, 2003; http://webbook.nist.gov.

(33) *ICT Thermodynamic Code*, version 1.0: Frauenhofer-Institut für Chemische Technologie (ICT): Pfinztal/Berghausen, Germany, 1988−2000.